perimental Investigation of the Compressible Free Mixing of Two Dissimilar Gases," *AIAA Journal*, Vol. 4, No. 11, Nov. 1966, pp. 2017–2025.

[11] Shirie, J. W. and Seubold, J. G., "Length of the Supersonic Core in High Speed Jets," *AIAA Journal*, Vol. 5, No. 11, Nov. 1967, pp. 2062–2064.

[12] Eggers, J. M., "Velocity Profiles and Eddy Viscosity Distributions Downstream of a Mach 2.22 Nozzle Exhausting to Quiescant Air," TN D-3601, Sept. 1966, NASA.

[13] "Studies Pertaining to Bambi Ballistic Missiles–Plume Wind-Tunnel Research Program," ZR-AP-061-24, April 1962, General Dynamics Astronautics, San Diego, Calif.

[14] "Summary Report Rocket Exhaust Impingement Study," TR E 1-67, Nov. 1968, FMC Corp., Northern Ordnance Div., Minneapolis, Minn.

[15] Van Driest, E. R., "The Problem with Aerodynamic Heating," *Aeronautical Engineering Review*, Oct. 1956, pp. 26–41.

[16] Jepps, G. and Robinson, M. L., "Convective Heating at the Deflecting Surface of a Rocket Launch-Pad," *Journal of the Royal Aeronautical Society*, July 1967, pp. 469–475.

[17] Fay, J. A. and Riddell, F. R., "Theory of Stagnation Point Heat Transfer in Disassociated Air," *Journal of Aerospace of the Sciences*, Vol. 25, No. 2, Feb. 1958, pp. 73–85.

[18] Thring, M. W. et al., *Combustion and Propulsion*, Pergamon Press, New York, 1958.

[19] Brown, B. and McArty, K. P., "Particle Size of Condensed Oxides from Combustion of Metalized Solid Propellants," *Eighth Symposium (International) on Combustion*, Williams and Wilkins, Baltimore, Md., 1962, p. 817.

APRIL 1970 J. SPACECRAFT VOL. 7, NO. 4

A Theory for Base Pressures on Multinozzle Rocket Configurations

J. P. Lamb,* K. A. Abbud,† and C. S. Lenzo‡
The University of Texas at Austin, Austin, Texas

A new analysis is given for turbulent base flowfields in multi-nozzle configurations. The specific case of adiabatic flow in a four-nozzle symmetrical ring cluster is considered. Inviscid plume boundaries are described approximately with circular arcs. Because of symmetry, viscous effects at the common plume confluence can be treated by a planar analysis and flow conditions at the origin of the reverse jet thereby determined. The reverse jet development is analyzed with an integral method, using an effective eddy viscosity which is related to that in the free shear layers at the plume boundaries. The base pressure distribution is determined from the reverse jet impingement on the base plane. Depending upon the nozzle height, both weak and strong interactions may occur. Results of the present analysis are in general agreement with cold flow test data for a wide range of geometric variables.

Nomenclature

b_r = radius of reverse jet at cutoff station
C = Crocco number, $u(2c_pT_0)^{-1/2}$
E_1 = $\int_0^1 \tilde{\varphi}(1 - C_r^2\tilde{\varphi}^2)^{-1}\, d(y/b_r)$
E_2 = $\int_0^1 \tilde{\varphi}^2(1 - C_r^2\tilde{\varphi}^2)^{-1}\, d(y/b_r)$
F_1 = $4(\ln 2)^2C_c^2(1 - C_c^2)/F_2$
F_2 = $r_m(1 - 0.25C_c^2)[1 + (2\ln F_3 + C_c \ln F_4)]/\ln(1 - C_c^2)$
F_3 = $(1 - 0.25C_c^2)/(1 - C_c^2)$
F_4 = $(1 + 0.5C_c)(1 - C_c)/(1 - 0.5C_c)(1 + C_c)$
h = height of nozzle exit above base plane
H = $(S/2)$ sec 45°, see Fig. 4
I_1 = $\int_{-\infty}^{\eta} \varphi(1 - C_2^2\varphi^2)^{-1}d\eta$
I_2 = $\int_{-\infty}^{\eta} \varphi^2(1 - C_2^2\varphi^2)^{-1}d\eta$
k = c_p/c_v
L = length of plume boundary, see Fig. 1
M = mach number
$\dot{M}$ = momentum flow rate, $\int \rho u^2 dA$
m = mass flow rate, $\int \rho u\, dA$
P_b = static pressure at edge of base = ambient pressure
P_{0B} = base plane pressure at vehicle center
P_p = base plane pressure distribution
R_n = radius of nozzle exit
R_{pm} = maximum radius of inviscid plume boundary, see Fig. 1
r = radius of reverse jet
S = center-to-center spacing of nozzles on base plane, see Fig. 6
u = longitudinal velocity
Y = transverse coordinate in free layer
Z = axial coordinate along vehicle centerline
Z_{pm} = axial location of R_{pm}, see Fig. 1
β, δ, γ = angles, see Fig. 3
ϵ = nozzle expansion ratio
η = $\sigma y/L$
θ = angle measured from nozzle wall, Fig. 1
σ = spread rate parameter for free layer
ϕ = reverse jet velocity, $\tilde{u}/\tilde{u}_c = \exp[-(\ln 2)(r/r_m)^2]$
φ = free layer velocity, u/u_2
ψ = angle of plume boundary, see Fig. 1
ω = angle of meridian plane, see Fig. 2

Subscripts

0 = stagnation conditions
2 = freestream at edge of inviscid plume
amb = ambient
c = reverse jet centerline, see Fig. 5
d = dividing streamline of free layer
e = end of nonisobaric jet, see Fig. 5
i = nozzle exit
j = jet boundary streamline of free layer
m = average velocity in reverse jet

Presented as Paper 69-570 at the AIAA 5th Propulsion Joint Specialist Conference, U.S. Air Force Academy, Colo., June 9–13, 1969; submitted May 21, 1969; revision received January 27, 1970. This research was partially sponsored by NASA under Contract NAS 8-20321 with Marshall Space Flight Center.

* Associate Professor of Mechanical Engineering. Member AIAA.
† Research Engineer.
‡ Research Engineer. Member AIAA.

n = nozzle parameter
r = cutoff station
$(\tilde{\ })$ = reverse flow

Introduction

INTERACTIONS between exhaust plumes of clustered rocket nozzles can lead to relatively large pressures and extremely high heating rates on the vehicle base. Experimental investigations[1-3] have illuminated many features of multi-nozzle base flows and have provided sufficient design information so that the detrimental effects of base heating have been largely avoided in operational vehicles.[4] However, the evolution of analytical methods for predicting the effect of plume interactions on the base flow has not kept pace with the development of testing techniques and acquisition of data. Furthermore, previous theoretical treatments[5-8] have been dependent upon the inherent limitations of their component analyses.

The present paper presents a new theoretical model for these complex base flows, with emphasis on fluid dynamic aspects, viz., the determination of base pressure as a function of ambient pressure P_b and nozzle geometry, which includes height above the base h, lateral spacing S, and expansion ratio ϵ. Although the concepts of the present analysis are equally applicable to other multi-nozzle configurations, the particular geometry to be considered is the so-called "ring cluster" in which the nozzles are arranged around the periphery of a circle. Equations will be developed and numerical results presented for the specific case of a four-nozzle symmetrical cluster for which considerable cold flow test data are available.[1]

As implied above, the complete base flow model is composed of a number of component analyses which are classified in three categories: 1) inviscid plume effects, 2) viscous flow at the plume boundaries which results in a reverse jet, and 3) impingement of the jet on the vehicle base.

Inviscid Plume Impingement

The initial step in the analysis is a determination of inviscid boundaries for the exhaust plumes. Although a precise calculation can be made with the method of characteristics, a less accurate estimation can be justified in the current case because of the subsequent requirement for only a limited amount of information. Specifically, the required data must include only the boundary Mach number and flow direction and, in addition, must extend only for a short distance along the boundary surface to the plane of impingement with adjacent plumes

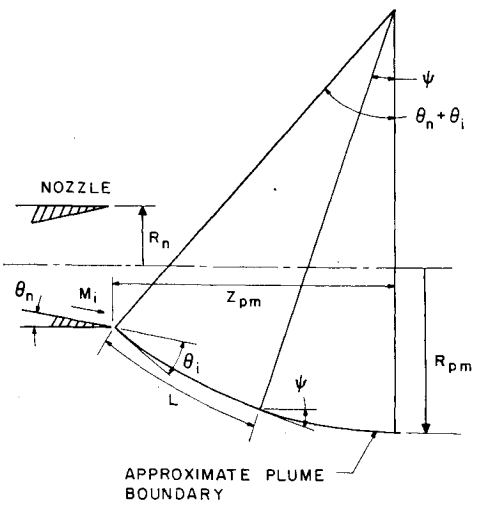

Fig. 1 Inviscid jet boundary approximation.

For the present, the well known circular arc approximation, developed by Love[9] and others, is utilized to estimate the flow direction. In this computation scheme the initial portion of the jet boundary is estimated with a circular arc which passes through the nozzle lip at the proper angle as well as through the point of maximum plume diameter (Fig. 1).

The present calculations were made using the semiempirical relations of Lord[10] which give the maximum plume radius R_{pm} and its axial location Z_{pm} in the form

$$\frac{R_{pm}}{R_n} = \frac{(P_i/P_b)^{1/2}(100 + 35M_i \tan\theta_n)}{15 + 60k_i - (4M_i - 6)(5 - 3k_i)(1 - 5\tan\theta_n)} \quad (1)$$

$$\frac{Z_{pm}}{R_n} = \frac{896(P_i/P_b)^{1/2}(6 + M_i)^{-1}M_i}{70 + 9k_i + 14(9k_i - 10)\tan\theta_n} \quad (2)$$

A quadrant of the flowfield for a four-nozzle cluster configuration is sketched in Fig. 2. It is observed that each pair of adjacent plumes impinges along a plane (JKBL) midway between the nozzles. Within each plane there is a line of impingement, denoted as BL. Also shown in Fig. 2 is a typical streamline S_2 at the plume boundary. This streamline lies in a meridian plane (OHGF), which passes through the nozzle centerline and is inclined to the impingement plane at an angle ω. It is observed that streamline S_2 impinges at an angle ψ_2 to the reference line HG, which is parallel to the rocket centerline KB. Streamline S_2 passes through a centered-wave§ (Prandtl-Meyer) compression and emerges as streamline S_3 in the impingement plane. The objective of this portion of the analysis is to estimate the velocity vector associated with streamline S_3. This will permit a determination of the downstream pressure, which is required in the calculation of the reverse jet.

It is also observed in Fig. 2 that there are two types of recompressions, depending on the angle of the meridian plane. For all points along an impingement line except the common point B, the only geometric restriction on S_3 is that it lie in the impingement plane. In general it will not lie in the meridian plane which contains S_2. However, at point B, the common intersection of all plumes, there must exist a second compression process which turns S_3 to the axial direction.

Some velocity vectors in that portion of the flowfield near the impingement point G are shown on an enlarged

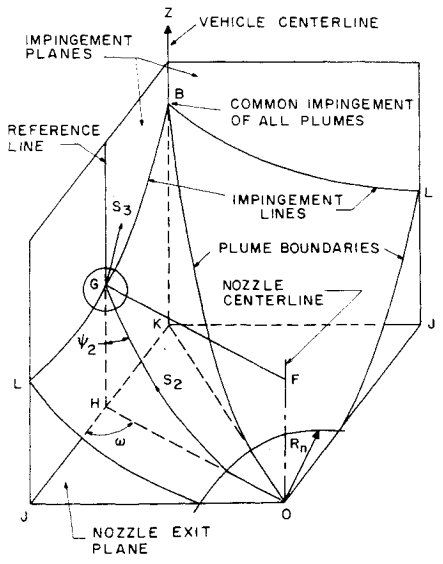

Fig. 2 Quadrant of inviscid flowfield.

§ It is known that pressure changes in the inviscid flow adjacent to a viscous layer do not occur abruptly as in an oblique shock.[11]

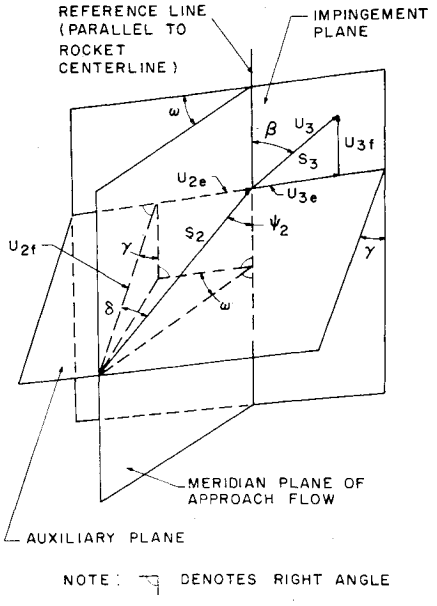

Fig. 3 Flow details near plume impingement.

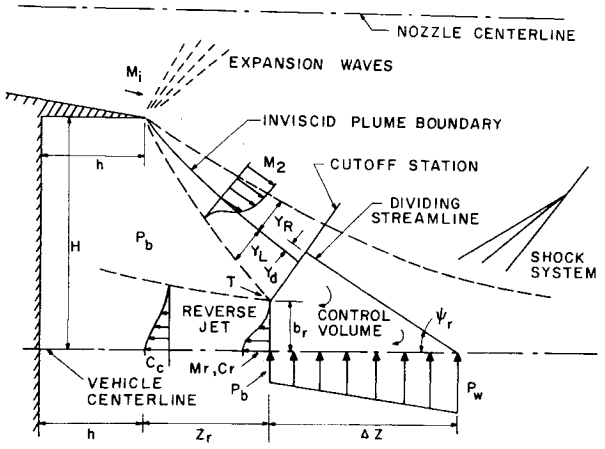

Fig. 4 Flow pattern in 45° meridian plane.

scale in Fig. 3. Besides impingement and meridian planes, Fig. 3 depicts a third plane which contains S_2 and is oriented such that its intersection with the impingement plane is perpendicular to the rocket centerline. It is seen that this plane makes an angle γ with the impingement plane. The velocity u_2 of streamline S_2 can be resolved into orthogonal components, u_{2e} which is parallel to the impingement plane and is unaffected by the recompression, and u_{2f}, which is modified as it turns through the angle γ. The components of the emerging streamline S_3 are given by $u_{3e} = u_{2e}$ and $u_{3f} = u_{3f}(\gamma, u_{2f})$. The value of u_{3f} (or M_{3f}) can therefore be determined from the Prandtl-Meyer compression of M_{2f} through the angle γ, which is given by $\gamma = \arccos(\cos\psi_2/\cos\delta)$ where $\delta = \arcsin(\sin\psi_2 \cos\omega)$.

Hence, for a known value of the impingement angle ψ_2 and any given value of ω, the value of γ can be determined. Knowing the two components of S_3, one can find M_3 as well as β from the relation $\beta = \arctan(u_{3e}/u_{3f})$, and P_3 can be found from the isentropic equation $P_3/(P_0)_i = P/P_0$ for M_3.

The downstream pressure for the common impingement point B in Fig. 2 can be estimated by considering two compressions in series, although in reality they occur simultaneously. One can obtain the axial Mach number M_4 from a second Prandtl-Meyer compression using the values of M_3 and β found from the foregoing relations for a value of $\omega = 45°$. Then

$$P_4/(P_0)_i = (P/P_0)_{M_4} \tag{3}$$

If one calculates the variation of P_3 along the line LB of Fig. 2 as well as the value of P_4 at point B, it is found that $P_4 \approx 3P_3$. Furthermore, the subsequent analysis of viscous effects indicates that the intensity of the reverse jet is proportional to the value of downstream static pressure. These conditions suggest that the recompression process at the rocket centerline is the dominant mechanism in determining the reverse jet flow. This means that viscous interaction effects are concentrated in the 45° meridian plane which passes through the common plume impingement point. In addition, because of symmetry and the relatively small size of the viscous regions, one can justify the use of a planar formulation of the viscous interaction process in the vicinity of the common impingement.

Viscous Flow Effects

It is well known that a portion of the free shear layer, which develops at the plume boundary, is unable to negotiate the relatively high pressure at the point of plume impingement. Because it cannot pass downstream, this low-speed portion of the shear layer is therefore reversed and returns to the base plane in the form of a jet.[3] Figure 4 depicts the flow pattern in the 45° meridian plane and illustrates the three major viscous flow components, viz., an isobaric free shear layer, a recompression region, and the reverse jet. Analyses of each of these components are presented in this section.

The turbulent mixing zone at the plume boundary is described with the well known analysis of Korst which has seen widespread application to various axisymmetric configurations including both underexpanded jet plumes[12] and internally converging base flows.[13] The integral method of Korst superimposes an asymptotic velocity profile onto the inviscid jet boundary. Allowance is made for the approximate nature of the profile by a slight lateral adjustment of its position on the boundary, the amount of adjustment being determined with the integral momentum equation. Mass fluxes within the mixing zone are determined with the integral continuity equation.

The usual error function profile $\varphi = \frac{1}{2}(1 + \text{erf}\eta)$ is utilized to characterize velocities in the shear layer. Use of these fully developed profiles implies that initial boundary layer effects are negligible. This is reasonable in the case of underexpanded jet plumes which originate from large-angle expansions at the nozzle lip. Such large turning angles are known to substantially eliminate most initial profile distortion.

A primary feature of the planar base pressure analysis of Korst and its axisymmetric applications by Bauer[12] and Mueller[13] is the use of an escape criterion which provides the necessary closure condition. In its initial formulation this reattachment model implied that the dividing streamline was isentropically stagnated to the static pressure downstream of the inviscid recompression. It was later found experimentally that the stagnation process was much more complex than suggested by this model and, in addition, that dividing streamline reattachment occurred at a pressure less than the downstream static pressure.

The problem of turbulent reattachment in a planar base flow has been analyzed by Lamb and Hood,[11] who found that accurate predictions could be made by utilizing the escape criterion as a means of identifying the dividing streamline rather than as a thermodynamic specification of the stagnation process. Therefore, in the present flow model the velocity along the dividing streamline in the shear layer is found by $\varphi_d^2 = C_d^2/C_2^2$, where $C_d^2 = 1 - (P/P_0)_d^{1-1/k}$ and $(P/P_0)_d = P_4/(P_0)_i$ from the inviscid analysis, Eq. (3). The Crocco number C_2 corresponds to the inviscid boundary Mach number M_2. The above value of φ_d allows one to determine the location (η_d) of the dividing streamline using the velocity profile.

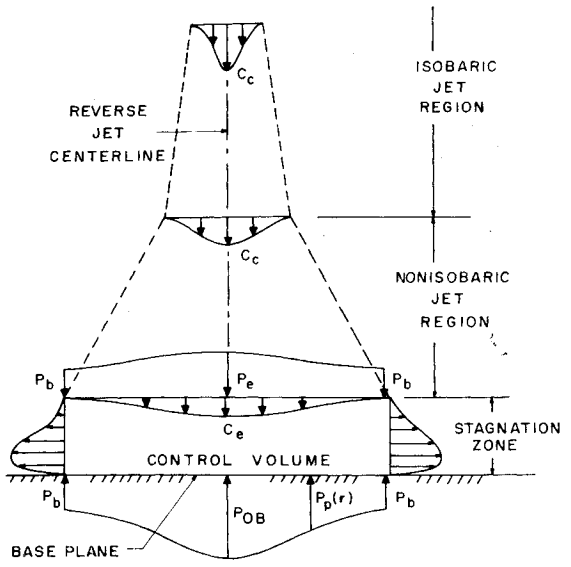

Fig. 5 Nonisobaric jet stagnation.

The effective edges of the shear layer must be specified for the recompression analysis. For the error function profile, which approaches its limiting values asymptotically, one must choose finite values for η to represent the effective width. In the present case $\eta_R = 2.5$ was chosen for the inner edge where $u = u_2$ and $\eta_L = -1.6$ for the outer edge where $u \approx 0$. The over-all predictions of the theory were not sensitive to η_R and η_L.

The physical locations of the shear layer outer edge and the dividing streamline can be obtained from the relations $Y_d = (L/\sigma)(\eta_d - \eta_m)$ and $Y_L = (L/\sigma)(\eta_L - \eta_m)$. The length of the shear layer along the inviscid boundary (see Fig. 1) is given by $L = Z_{pm}(\theta_n + \theta_i - \psi)\, csc(\theta_n + \theta_i)$, and the distances Y_d and Y_L are measured normal to the local slope ψ of the inviscid boundary. The quantity η_m, which gives the lateral displacement of the approximate profile, is also a function of L and ψ as well as C_2. The expression for η_m has been omitted for brevity but can be found elsewhere.[12,13]

As the fluid in the free layer approaches the point of inviscid plume impingement, it will interact with the reverse flow. The point of initial interaction is denoted as the "cutoff station"; it marks the beginning of the recompression region and is determined from the following physical conditions. The zero-velocity edges of both the freelayer and reverse flow profiles must coincide (point T, Fig. 4), and the mass flux in the mixing layer below the dividing streamline must equal that in the reverse jet half-width.

As was noted earlier, flow in the 45° meridian plane can, because of symmetry, be considered as a planar flow of infinitesimal width. It is therefore possible to utilize the reattachment analysis of Lamb and Hood[11] to estimate conditions in the reverse jet at the cutoff station. This is done through an application of continuity and momentum equations to the control volume shown in Fig. 4. The former appears as

$$C_r E_1 = (C_2 I_{1d}/\sigma)(L_r/b_r) \tag{4}$$

while the momentum expressions for the axial and transverse directions can be combined in the form

$$\frac{b_r}{R_n}\left[1 + \frac{2k}{k-1} C_r^2 E_2\right] - \left[1 + \frac{P_w}{P_b}\right]\frac{\Delta Z}{2R_n}\tan\psi_r + \frac{L}{\sigma R_n}\left[\eta_d - \eta_L + \frac{2k}{k-1} C_2^2 I_{2d}\right]\sec\psi_r = 0 \tag{5}$$

In determining mass and momentum fluxes for the reverse flow, a Gaussian distribution has been employed, i.e., $\tilde{\varphi} = \tilde{u}/\tilde{u}_r = \exp[(-2.5\ \ln 2)(y/b_r)^2]$. In addition, b_r and ΔZ are given by $b_r = H + Y_L \cos\psi_r - Z_{pm}\csc(\theta_n + \theta_i)\cos\psi_r - \tan(\theta_n + \theta_i)$ and $\Delta Z = b_r \cot\psi_r + (Y_d - Y_L)\csc\psi_r$. The reader is referred to the preprint and to Ref. 11 for further details of the development and for a discussion of one solution technique for the two unknowns P_w and L_r. The parameter L_r is of primary importance here, because it locates the end of the free layer along the plume boundary and allows one to determine the reverse jet parameters C_r and b_r, which become the initial conditions for the reverse jet calculation.

Although the foregoing interaction analysis determined jet parameters only in the two 45° meridian planes, it is recognized that the jet will be nearly circular from the outset and that the asymmetry would tend to decay rapidly.[14] It is thus possible to utilize the jet analysis developed by Donaldson and Gray[15] and others.

The present application requires consideration of only the decaying-jet regime wherein the centerline velocity decreases with development distance and the velocity profiles are similar. The jet development can be determined through a simultaneous solution of two momentum integral relations, one for the complete jet and another for the inner core region. The latter equation includes the shear stress which largely governs the rate of growth of the jet.

Using a Gaussian distribution for the velocity profile one can integrate both momentum equations in closed form and, after combination, obtain a first-order differential equation for the decay of the centerline Crocco number C_c in the form

$$dC_c^2 = KF_1(C_c, r_m)dZ \tag{6}$$

where the function F_1 is given in the Nomenclature. The characteristic radius of the jet r_m is given by $r_m^2 = (r_m)_r^2 \ln(1 - C_r^2)/\ln(1 - C_c^2)$ where C_r^2 and $(r_m)_r = 0.4b_r$ are found from the previous reattachment analysis. The parameter K in Eq. (6) comes from the eddy viscosity formulation employed by Donaldson and Gray.

Although Eq. (6) could be integrated to yield the longitudinal variation of C_c^2, it is more expedient merely to use a finite difference form and compute incremental changes in C_c^2 while marching from the cutoff station toward the base plane. An increment in Z as large as $0.1(r_m)_r$ yields reasonable accuracy. Once C_c^2 is determined, all jet parameters can be evaluated.

A reasonable specification of the shear stress parameter K proved to be a difficult task. Initial computations were made using the variation of K with M_m which was given by Donaldson and Gray. However, the resulting distributions of base-plane pressure exhibited only qualitative agreement with test data, thus suggesting that there were significant differences between the growth rate of the reverse jet and that in typical jets. This situation is not completely unexpected, inasmuch as fluid in the reverse jet must first traverse the turbulent mixing zones at the plume boundaries. The following method has been devised in an attempt to relate the stress level in the reverse flow to that in the shear layer.

It has been shown by Chow and Korst[16] that the maximum eddy viscosity in a free shear layer occurs at the jet boundary streamline which is near the center of the layer. This eddy viscosity is given by $(\rho\epsilon)_j = [\rho u T/T_0]_2(L_r/\sigma^2)\pi^{1/2} I_{2j} \exp(\eta_j)$.[2] At the cutoff station the corresponding value of $\rho\epsilon$ at the half-radius of the reverse jet is $(\rho\epsilon)_r = \frac{1}{2}K_r[\rho\tilde{u} r_m T/T_0]_r/(1 - 0.25C_r^2)$. In view of the conclusion[17] that $\rho\epsilon$ is nearly constant in compressible free viscous flows, the foregoing values of $\rho\epsilon$ can be equated and an estimate of K_r obtained. The variation of K for the remainder of the decaying jet is assumed to be equivalent to that presented by Donaldson and Gray, viz., $K = K_r[1 + \exp(-4C_c^2)]$. Base pressure results obtained with this improved specification of K were much more realistic. However, some disagreement

persisted, because K_r was insensitive to the lateral spacing of the nozzles on the base plane.

The final specification for K_r was therefore

$$K_r = [C(I_{2j}/\sigma^2)\exp(\eta_j^2)]_{M_2}(2\pi^{1/2})(1 - C_e^2)L_r/(4r_{ef}C_r)$$

where $r_{ef} = (r_m)_r$ evaluated for the nozzle spacing $S/R_n = 3.5$. The expression for K_r is regarded as tentative and somewhat speculative. However, it is believed that there is sufficient rationale in the derivation to justify its usage for similar nozzle geometries until experimental information on the reverse jet stress level becomes available.

Reverse Jet Impingement

The pressure distribution[3,5] on the base plane exhibits a maximum at the rocket centerline which is characteristic of velocity profiles of near-Gaussian form. It has been shown by Barnes and Sullivan[18] that the wall pressure distributions for such jet impingements are also nearly Gaussian. The relation between the wall pressure P_p and the jet velocity profile ϕ can be expressed as

$$\ln\{[P_p(r) - P_b]/(P_{0_B} - P_b)\} \approx 0.8\ln\phi \qquad (7)$$

where P_{0_B} is the maximum impingement pressure at the vehicle centerline; P_{0_B} may be taken as the characteristic base-plane pressure for multinozzle configurations, and variations in P_{0_B} with altitude and base geometry can be employed to portray the over-all process.

It is seen in Fig. 7 that there are two general types of variations of P_{0_B} with altitude for a given nozzle ϵ and S. The two distributions are primarily dependent upon the height h of the nozzle exit above the base plane. For long nozzles there is a gradual increase in P_{0_B} over P_b as P_b is lowered. In some instances a further decrease in P_b results in a sharp peak in the P_{0_B} distribution. Conversely, for short nozzles there is a relatively high, almost constant value of P_{0_B} over a wide range of P_{amb}.

Because of the similarity with conventional base flow,[13] the nearly uniform distribution of P_{0_B} for short nozzles has often been interpreted as an indication of choking in the vent area between nozzles. However, the reverse jet mass flow rates determined with the present model were found to be sufficiently small that the occurrence of choking appears to be highly unlikely.

The foregoing result suggests that each of these general types of pressure distributions corresponds to a particular jet impingement process. For long nozzles the process is weak because the jet itself is largely unaffected. In the case of short nozzles there is a long interaction length, and the reverse jet becomes nonisobaric; this is considered to be a strong interaction.

For weak impingement the peak pressure on the base plane can be determined from simple relations for one-dimensional stagnation. For $M_c < 1$ in the approaching jet, the isentropic relation can be employed. For $M_c > 1$, the isentropic equation yields values of P_{0_B} which are far too large. This suggests that further dissipation, in addition to that in the jet development, occurs during stagnation. The simplest type of irreversible stagnation is that of a normal shock. It was found that this model yielded realistic values for P_{0_B} when $M_c > 1$. This computation does not imply that a normal shock actually exists[5] but merely that the stagnation process at the centerline possesses nearly the same degree of irreversibility as a normal-shock stagnation.

In the strong-interaction stagnation process, the relatively high pressures in the base plane are propagated upstream through the jet and result in a more rapid decay of centerline velocity than would occur in an isobaric flow. Although a comprehensive analysis of such nonisobaric jets was not justified in the present context, it was found that reasonable estimates of the base plane pressure could be obtained with the following model: the jet contains a distinct zone of rising pressure which lies between the isobaric region and a stagnation zone immediately adjacent to the base (Fig. 5). Because the length of the nonisobaric region is unknown, it is assumed that P increases over a sufficiently short distance that a) shear stress effects can be omitted and b) the jet mass flux is nearly constant. These simplifications allow the nonisobaric region to be described with the usual integral equations of continuity and momentum.

For ease of computation the radial distribution of static pressure is taken to be equivalent to the Gaussian velocity profile. The pressure therefore varies from P_c at the centerline to ambient (P_b) at the outer edge according to the relation $P = P_b + (P_c - P_b)\phi$.

The over-all momentum equation for the nonisobaric region can be written as

$$\int_0^\infty (P - P_b + \rho\tilde{u}^2)dr^2 = \text{const} \qquad (8)$$

while the appropriate continuity relation is

$$\dot{m} = \int_0^\infty \rho\tilde{u}dr^2 = \text{const} \qquad (9)$$

As in the isobaric jet analysis, these equations can be normalized with parameters at the jet centerline and with the radius r_m. After introduction of velocity, density, and static pressure profiles, the resulting integrals can be evaluated in closed form so that Eqs. (8) and (9) can be evaluated at each end of the nonisobaric region and combined to yield

$$\frac{P_e - P_b}{P_b} = \frac{C_e(\ln A_c \ln B_e - \ln A_e \ln B_c)}{(1 + 1/k)C_e \ln B_c - \ln A_c \ln A_e + \ln B_c \ln B_e} \qquad (10)$$

where $A = 1 - C^2$, $B = (1 - C)/(1 + C)$, and the subscript e refers to conditions at the beginning of the stagnation zone.

Because both P_e and C_e are unknown in Eq. (10) an additional relationship is required to close the solution. This is provided by a control volume analysis of the stagnation zone in Fig. 5. At the base plane the pressure distribution s given by Eq. (7) while at the upper control surface, displaced from the base by a small but unspecified distance, the flow conditions are those of the nonisobaric jet given previously.

A momentum balance for the control volume can be written as

$$\int_0^\infty (P - P_p)dr^2 = -\int_0^\infty \rho\tilde{u}^2 dr^2$$

where P and $(\rho\tilde{u}^2)$ refer to distributions in the nonisobaric jet. After normalization as before and insertion of the Gaussian profiles, the foregoing equation can be integrated to yield

$$\frac{P_{0_B} - P_b}{P_b} = -\frac{k}{k-1}\ln(1 - C_e^2) - \frac{P_e - P_b}{P_b}\left[\frac{k+1}{k-1} + \frac{k}{k-1}\frac{1}{C_e}\ln\frac{1 - C_e}{1 + C_e}\right] \qquad (11)$$

Substitution of Eq. (10) into Eq. (11) yields the final expression for P_{0_B} as a function of C_c and C_e. However, because C_e is not known a priori, the necessary uniqueness of the solution is provided by requiring that P_{0_B} determined from the foregoing integral model be equal to P_{0_B} found from a normal-shock stagnation of C_e, since $M_e > 1$ always.

Because no interaction lengths have been specified, the appropriate values of C_c at the end of the isobaric region are also unknown. It was found that little error is incurred by choosing the hypothetical value of C_c which would exist if the isobaric jet developed all the way to the base plane as in the weak interaction case.

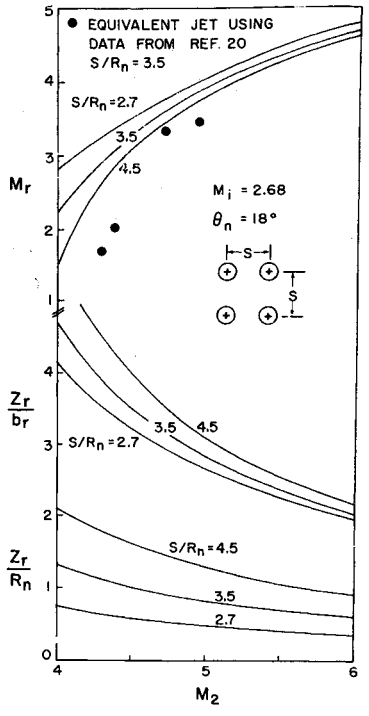

Fig. 6 Variation of reverse jet parameters M_r, Z_r/b_r, and Z_r/R_n.

Discussion of Typical Results

Because there are many components of the present flow model, it is desirable to summarize the over-all calculation procedure. Known information includes ϵ (or M_i), θ_n, h/R_n, and the center-to-center distance between nozzles on the base plane (S/R_n). A value of ambient pressure (P_b) is first chosen and the corresponding inviscid plume boundaries determined. The maximum static pressure P_4 downstream of inviscid plume impingement can then be found from Eq. (3). This makes possible the identification of the dividing streamline, from which input data for the momentum balance of Eq. (5) can then be determined. The solution technique of Ref. 11 allows one to determine the proper value of L_r and the reverse jet parameters C_r^2 and $(r_m)_r$ at the cutoff station using Eq. (4).

Development of the reverse jet is determined with Eq. (6). The correct values of C_c and r_m, which are required in the impingement calculation, are found by allowing the isobaric jet to develop to the base plane. For weak impingement ($h/R_n > 0.5$), P_{0B} is found from isentropic or normal-shock relations, depending on whether the final value of M_c is greater or less than unity. For short nozzles Eqs. (10) and (11) along with the normal-shock equation are employed to determine P_{0B}. Finally, the distribution of base-plane pressure can be found from Eq. (7).

Although the present flow model does not indicate which type of interaction would occur in general, experiments[1] suggest that the maximum possible value of P_{0B} can be determined using the strong interaction model with zero nozzle height. Subsequent values of P_{0B} from the weak interaction impingement cannot exceed this maximum value.

The only parameter unspecified in the foregoing discussions is the spread rate parameter σ of the turbulent free layer. The present numerical results incorporate a theoretical ariation of σ with M_2 which has been shown[19] to be in reasonble agreement with available experimental results.

Because of the extreme significance of the reverse jet in establishing the base-plane pressure distribution (and hence heating rate), some typical results at the origin of the jet (i.e., at the cutoff station) are shown in Fig. 6 for one value of M_i and three values of S/R_n. It will be recalled that h does not enter this calculation. The variation of centerline Mach number M_r with plume Mach number M_2 is shown in the upper part of Fig. 6; M_r decreases with increased S/R_n, although the effect is rather small due to the increased width of the free layers for larger values of S/R_n.

Shown also in Fig. 6 are M_r values developed from the recent experimental data of Brewer and Craven.[20] Their measurements indicated M_r's on the order of unity but at a $P_r \gg P_b$. These values cannot be compared directly with the predictions of the present model which assumes P_b at the cutoff station. However, one can compare the current predictions with values of M_r for an "equivalent jet" having the same total momentum flux, same size, and the same velocity profile as the actual jet but which exists at P_b. Under these conditions one can show that $\dot{M} \propto P \ln(1 - C_r^2)$. Thus, the equivalent M_r is found from $\ln(T/T_0)_{Mr} = (P_s/P_b) \ln(T/T_0)_{M\text{exp}}$ where P_s and M_{exp} are experimental values of local pressure and M_c. The M_r values obtained in this manner are in reasonable agreement with the predicted values (Fig. 6). The remaining discrepancies are attributed to differences between the actual three-dimensional jet impingement process and the highly simplified planar model of Lamb and Hood.

Further inspection of Ref. 20 shows that the reverse jet, in addition to the lower M_c, is nonisobaric over a wider range of conditions than is postulated in the present analysis. However, near the base plane, M_c's predicted by the current

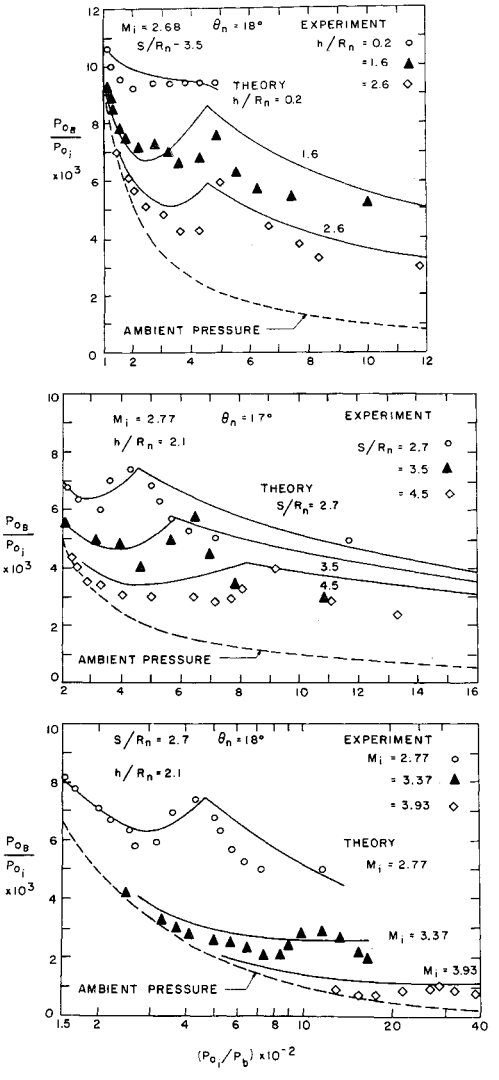

Fig. 7 Variation of centerline base pressure P_{0B} with reciprocal of ambient pressure, illustrating effects of nozzle height (top), lateral spacing of nozzles (middle), and nozzle expansion ratio (bottom).

isobaric jet decay are in reasonable agreement with those which occur in the actual nonisobaric jet.

Figure 6 also illustrates the variations of the axial location Z_r and radius b_r of the reverse jet at the cutoff station. The effect of nozzle spacing is proportionally the same for both jet parameters so that their ratio is, in common with M_r, only slightly affected by S/R_n. Figure 6 thus indicates that, for increasing nozzle spacing, Z_r/b_r increases while M_r decreases, both of which tend to reduce P_{0_B}.

Figure 7 depicts the variation of P_{0_B} with $(P_{\text{amb}})^{-1}$, which is proportional to altitude. Both pressures are normalized with P_{0_i}, which is taken as a constant. The corresponding variation of P_{amb} is also presented for comparison. The upper portion of Fig. 7 illustrates the effect of nozzle height (h/R_n) for both short and long nozzles, i.e., both strong and weak impingements at the base plane. The characteristic peak in the P_{0_B} variation is predicted for the weak impingement, and the general agreement with experimental results[1] is reasonably good. The present analysis suggests that there is no particular physical significance to the flow processes in the vicinity of the peak, which occurs because the variations of b_r, Z_r, and M_r with altitude result in reverse jets with quite different growth rates.

The effect of nozzle spacing on the base plane pressure is shown in the midpart of Fig. 7. It is seen that, as S/R_n increases, the peak occurs at a higher altitude. The same behavior can result by increasing M_i, as is illustrated in the lower part of Fig. 7. It is observed that predicted base pressure variations for the two higher Mach numbers do not exhibit peaks, whereas the test data indicate decreased but still observable excursions.

It can be concluded that, although the present predictions do not agree with measurements at every point, the over-all results are sufficiently close to suggest that the present flow model could serve as a basis for heat transfer predictions as well as for estimating the base flow processes for other multinozzle geometries.

References

[1] Goethert, B. H. and Matz, R. J., "Experimental Investigation of Base Flow Characteristics of Four-Nozzle Cluster-Rocket Models," *The Fluid Dynamic Aspects of Space Flight*, AGARDograph No. 87, Vol. 2, 1966, pp. 223–244.

[2] Sargent, R. J., "Base Heating Scaling Criteria for a Four-Engine Rocket Cluster Operating at High Altitudes," AIAA Paper 65-826, New York, 1965.

[3] Wasko, R. A. and Cover, T. L., "Experimental Investigation of Base Flow Fields at High Altitudes for Configurations of Four and Five Clustered Nozzles," TM X-1371, 1967, NASA.

[4] Etemad, G. A. and Korkan, K. D., "Base Flow Characteristics and Thermal Environment of Launch Vehicles with Strap-on Solid Rocket Motors," *Journal of the Astronautical Sciences*, Vol. 15, No. 1, 1968, pp. 5–13.

[5] Marion, E. D., Daniels, D. J., Herstine, G. L., and Burge, G. W., "Exhaust Reversal from Cluster Nozzles—A New Flow Model," Paper 2706-62, 1962, American Rocket Society, New York.

[6] Page, R. H. and Dixon, R. J., "Base Heating on a Multiple Propulsion Nozzle Missile," AIAA Paper 63-179, New York, 1963.

[7] Goethert, B. H., "Base Flow Characteristics of Missiles with Cluster-Rocket Exhausts," *Aerospace Engineering*, Vol. 20, No. 3, March 1961, pp. 28, 29, 108–117.

[8] Dixon, R. J. and Page, R. H., "Theoretical Analysis of Launch Vehicle Base Flow," *Separated Flows*, Conference Proceedings 4, May 1966, AGARD, pp. 919–940.

[9] Love, E. S., Grigsby, C. E., Lee, L. P., and Woodling, M. J., "Experimental and Theoretical Studies of Axisymmetric Free Jets," R-6, 1959, NASA.

[10] Lord, W. T., "On Axisymmetric Gas Jets," Aero 2626, July 1959, Royal Aircraft Establishment, England.

[11] Lamb, J. P. and Hood, C. G., "An Integral Analysis of Turbulent Reattachment Applied to Plane Supersonic Base Flows," *Transactions of the ASME, Ser. B*, Vol. 90, No. 4, Nov. 1968, pp. 553–560.

[12] Bauer, R. C., "Theoretical Base Pressure Analysis of Axisymmetric Ejectors without Induced Flow," TDR 64-3, Jan. 1964, Arnold Engineering Development Center, Arnold Air Force Station, Tenn.

[13] Mueller, T. J., "Determination of the Turbulent Base Pressure in Supersonic Axisymmetric Flow," *Journal of Spacecraft and Rockets*, Vol. 5, No. 1, Jan. 1968, pp. 101–104.

[14] Rom, J., "Study of Similarity of High-Temperature, Turbulent Jets," *AIAA Journal*, Vol. 6, No. 7, July 1968, pp. 1368–1370.

[15] Donaldson, C. duP. and Gray, K. E., "Theoretical and Experimental Investigation of the Compressible Free Mixing of Two Dissimilar Gases," *AIAA Journal*, Vol. 4, No. 11, Nov. 1966, pp. 2017–2025.

[16] Chow, W. L. and Korst, H. H., "On the Flow Structure within a Constant Pressure Compressible Turbulent Jet Mixing Region," TND-1894, 1963, NASA.

[17] Hill, J. A. F. and Nicholson, J. E., "Compressibility Effects on Fluid Entrainment by Turbulent Mixing Layers," CR-131, 1964, NASA.

[18] Barnes, D. A. and Sullivan, R. D., "Rotational Solutions of the Euler Equations," Rept. 79, Sept. 1965, Aeronautical Research Associates of Princeton, Princeton, N.J.

[19] Lamb, J. P. and Bass, R. L., "Some Correlations of Theory and Experiment for Developing Turbulent Free Shear Layers," *Transactions of the ASME, Ser. D*, Vol. 90, No. 4, Dec. 1968, pp. 572–580.

[20] Brewer, E. B. and Craven, C. E., "Experimental Investigation of Base Flow Field at High Altitude for a Four-Engine Clustered Nozzle Configuration," TN D-5164, 1969, NASA.